Supporting Information

Spectroscopic Evidence for 1,2-Diiminoethane – A Key Intermediate in Imidazole Synthesis

André K. Eckhardt*

Lehrstuhl für Organische Chemie II, Ruhr-Universität Bochum, 44801 Bochum (Germany); Andre.Eckhardt@rub.de

Table of Contents

Experimental Section

General remarks. NMR spectra were recorded on Bruker AVIII-300, AVIII-400 and DRX-400 spectrometers at 303 K. Chemical shifts (δ) are given in ppm relative to tetramethylsilane (TMS, δ = 0.00 ppm) as the internal standard or to the respective solvent residual peaks (DMSO: δ = 2.50 and 39.53 ppm; D_2O: δ = 4.79 ppm). GC-MS was carried out on an Agilent Technologies 7820 A gas chromatograph connected to an Agilent Technologies 5977B mass selective detector (EI, 70 eV), respectively, equipped with an Agilent J&W fused silica HP-5MS column (30 m × 0.25 mm × 0.25 µm). Conditions: helium carrier gas, 1.2 mL/min constant flow; injector temperature, 250 °C; source temperature, 230 °C; quadrupole temperature, 150 °C. GC oven temperature program: 60 °C isothermal, 2.5 min; 60 – 250 °C, 40 °C/min; 250 °C, 8.75 min. ESI-MS experiments were performed on an Advion Expression-L compact mass spectrometer.

Matrix isolation studies.[1] All matrix isolation infrared studies were performed on a Sumitomo RDK 408D2 closed-cycle refrigerator cold head powered by a Sumitomo CSW-71 compressor unit. The vacuum shroud was outfitted with transparent KBr windows and the sample holder mounted at the base of the cold head was outfitted with a polished CsI window transparent in the IR measurement range of 4000-400 cm^{-1}. The temperature on the sample holder was measured by a Si diode and could be adjusted by two resistive heating cartridges operated by a Lakeshore 336 temperature controller. All measurements were conducted at 3 K and an oil diffusion pump was employed to obtain a high vacuum of approximately 1 x 10^{-5} mbar at room temperature. The precursor molecule was dissolved in pump oil (Pfeiffer P3) and evaporated from a glass flask at 0-10 °C and co-condensed onto a CsI window at 12 K with a large excess of argon. The flow rate of the noble gas was set to 2.7 sccm with the help of an MKS mass flow controller and typically 1-1.5 mbar Ar min^{-1} was deposited onto the CsI window from a ~2.5 L silylated glass storage bulb over the course of an hour. Irradiation experiments were performed using an Osram HBO-200W high-pressure mercury lamp in an Oriel housing in combination with a 260–320 nm dichroic mirror or a Newport Model 77250 1/8m monochromator. For irradiation experiments with a wavelength of 254 nm we employed an Oase Vitronic 11 pool lamp (14 Watt). IR spectra were recorded using a Bruker IFS 66v/s spectrometer collecting 50 scans with a standard resolution of 0.5 cm^{-1} in the 4000–400 cm^{-1} region. For the UV/Vis spectroscopic experiments, a different matrix setup was used with the vacuum shroud equipped with quartz windows and a sapphire window attached to the cold head sample holder. In this case, cryogenic conditions were attained using a Sumitomo RDK 408D2 closed-cycle refrigerator cold head powered by a Sumitomo F70H compressor unit. The UV/Vis spectra were recorded using a PerkinElemer Lambda 1050 UV/Vis spectrometer. Spectra were recorded in the 190-800 nm range with a resolution of 1 nm and a scan speed of 266.75 nm min^{-1}. In the range of 190-320 nm a deuterium lamp was used as a light source and switched to a halogen lamp for wavelengths above 320 nm. For the combination of HVFP with matrix isolation we employed a homebuilt, water-cooled oven directly connected to the vacuum shroud of the cryostat. The pyrolysis zone consisted of an empty quartz tube (inner diameter 8 mm, length of heating zone 10 cm) resistively heated by a Thermocoax wire. The temperature was controlled by a Ni/CrNi thermocouple. At a distance of approximately 70 mm, all pyrolysis products were condensed on the surface of the matrix window at 12 K. For all experiments we used Ar of 99.999% purity.

Irradiation experiments. A solution of **4** (~10–40 mg) in 0.6 mL D_2O was irradiated for 4.5–7 h in a quartz NMR tube with an Osram HBO-500W high-pressure mercury lamp in an Oriel housing in combination with a 260–320 nm dichroic mirror. The average temperature of the irradiated solution was ~55 °C and the solution turned yellow after approximately one hour. The reaction mixture was analyzed by NMR spectroscopy and ESI-MS. For GC-MS studies the mixture was dried for 48 h at room temperature under the fume hood and the resulting brown solids diluted in CH_2Cl_2 (~1 mg ml^{-1}) and directly injected into the GC/MS instrument.

Quantum chemical calculations. For all geometry optimizations and frequency calculations the Gaussian16 program package was used.[2] The B3LYP[3-5] hybrid functional together with the 6-

311++G(2d,2p) basis set[6, 7] was employed for all geometry optimizations, infrared frequency calculations and time-dependent DFT[8-10] calculations for predicting vertical electronic excitation energies. Vibrational frequency calculations were used to characterize stationary points, obtain zero-point vibrational energy corrections and calculate harmonic infrared spectra for comparisons with the experiment. Transition states were characterized by exactly one imaginary frequency and analyzed by IRC calculations in forward and reverse direction. The complete basis set (CBS) energies were extrapolated from explicitly computed cc-pVTZ[11-13] and cc-pVQZ[11-13] single point energies utilizing the built-in extrapolation[14-16] routine in ORCA 5.0.3.[17] Initial conformational studies were performed using Grimme's xtb[18, 19] and CREST[20] program packages. All structures were visualized using Chemcraft.[21]

Synthesis

***CAUTION*:** Azides are highly energetic compounds with sensitivity towards heat and impact. Although we had no problem in synthesis, proper protective measures (safety glasses, face shield, leather coat, grounded equipment and shoes, Kevlar® gloves, and ear plugs) should be used when undertaking work involving these compounds.[22] While degassing, 1,2-diazidoethane exploded during thawing in a freeze-pump-thaw cycle. Therefore, we dissolved the compound in pump oil and performed our matrix isolation experiments with this diluted mixture.

1,2-Diazidoethane (4)

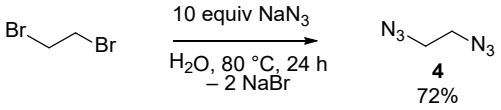

The compound was synthesized according to the procedure of Betzler *et. al*.[23] To a solution of sodium azide (2.6 g, 40 mmol) in water (15 mL) was added 1,2-dibromoethane (0.34 mL, 3.99 mmol) dropwise at room temperature. The solution was heated to reflux at 80 °C for 24 hours and extracted with ethyl ether (2 × 10 mL) and dried with magnesium sulfate. Due to the explosive nature of the compound, the organic solvent was evaporated at room temperature over the course of several hours under the fume hood to yield 320 mg (72 %) of a slightly yellowish liquid.

^{1}H NMR (300 MHz, DMSO-d_6): δ = 3.52 (s, 2 H, CH_2) ppm.
^{13}C NMR (76 MHz, DMSO-d_6): δ = 50.0 (CH_2) ppm.
IR: 2092 (vs).

1,2-Diazidoethane-d_4 (4-d_4)

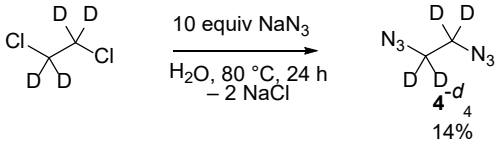

To a solution of sodium azide (3.25 g, 50 mmol) in water (20 mL) was added 1,2-dichloroethane-d_4 (515 mg, 5 mmol) dropwise at room temperature. The solution was heated to reflux at 80 °C for 24 hours and extracted with ethyl ether (2 × 10 mL) and dried with magnesium sulfate. Due to the explosive nature of the compound, the organic solvent was evaporated at room temperature over the course of several hours under the fume hood to yield 80 mg (14 %) of a slightly yellowish liquid.

^{1}H NMR (300 MHz, DMSO-d_6): δ = -
^{2}D NMR (300 MHz, DMSO): δ = 3.52 (s, 2 H, CD_2) ppm.
^{13}C NMR (101 MHz, DMSO-d_6): δ = 49.3 (p, CD_2, J = 22.1 Hz) ppm.
IR: 2092 (vs).

Infrared and UV/Vis Spectra

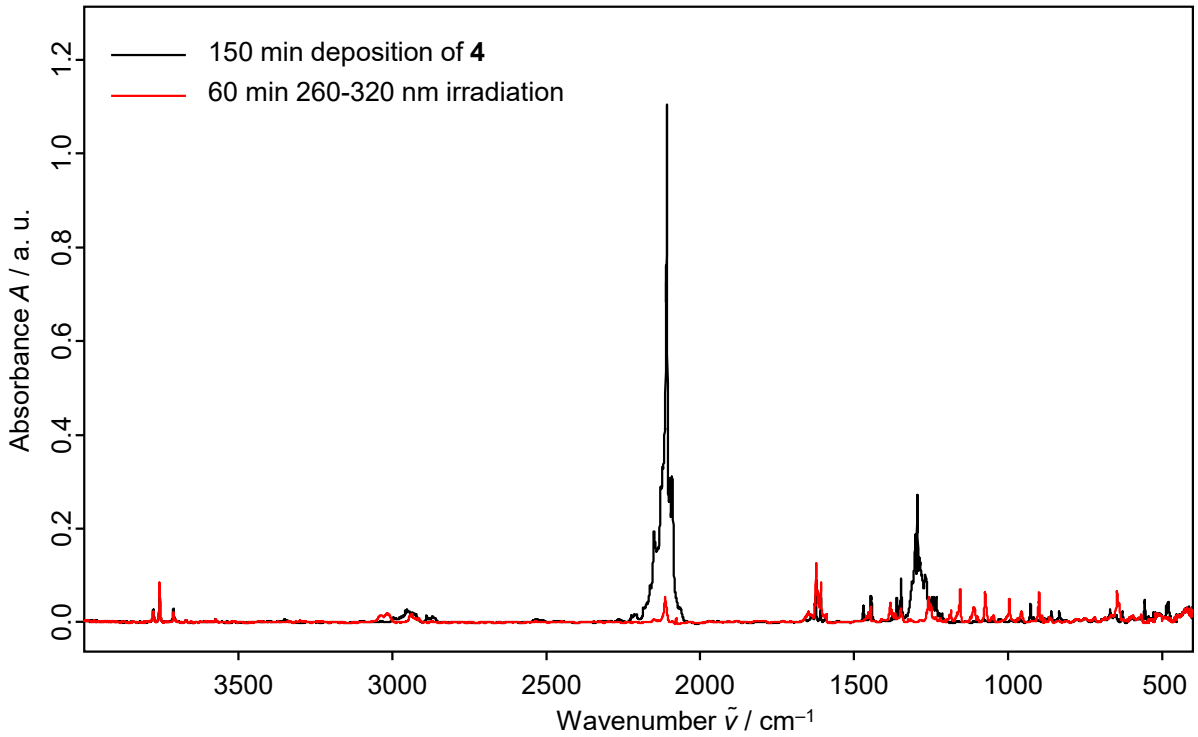

Figure S1: Black: IR-spectrum recorded after 150 min deposition of 1,2-diazidoethane (**4**) at 0-10 °C isolated in an excess of solid argon at 3 K; Red: Irradiation of the same matrix with UV light (λ = 260 – 330 nm) for 60 min.

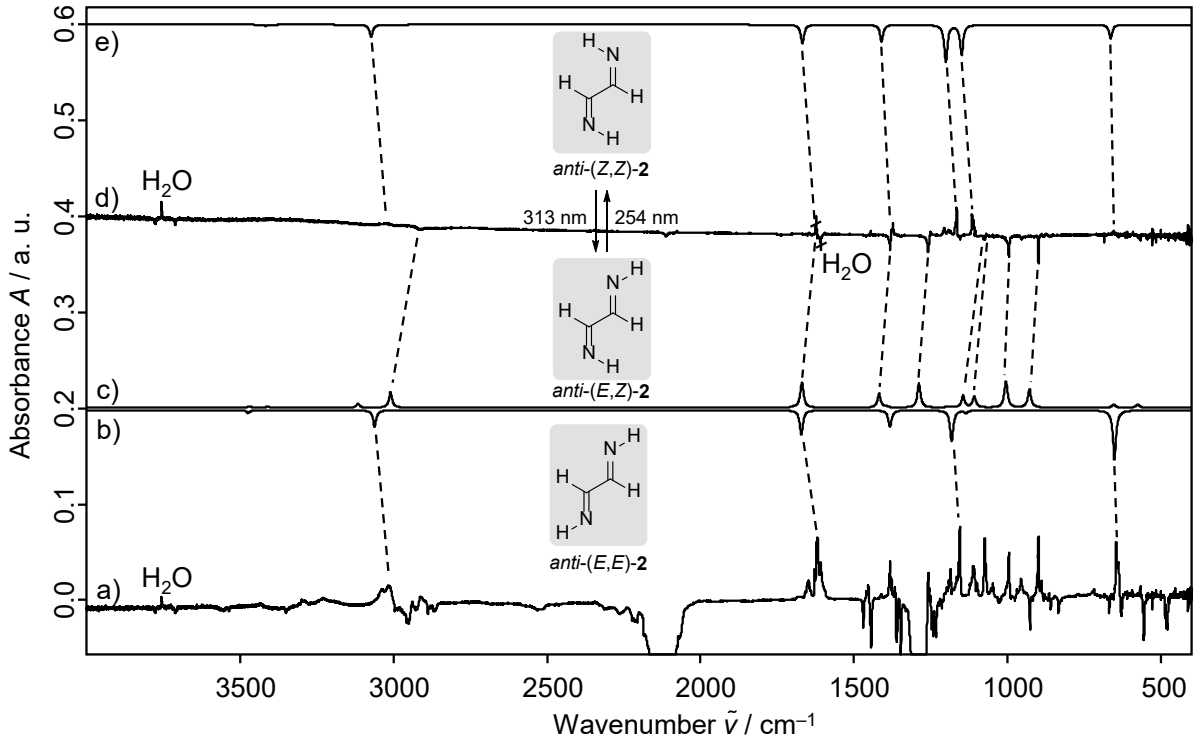

Figure 1 Extension.

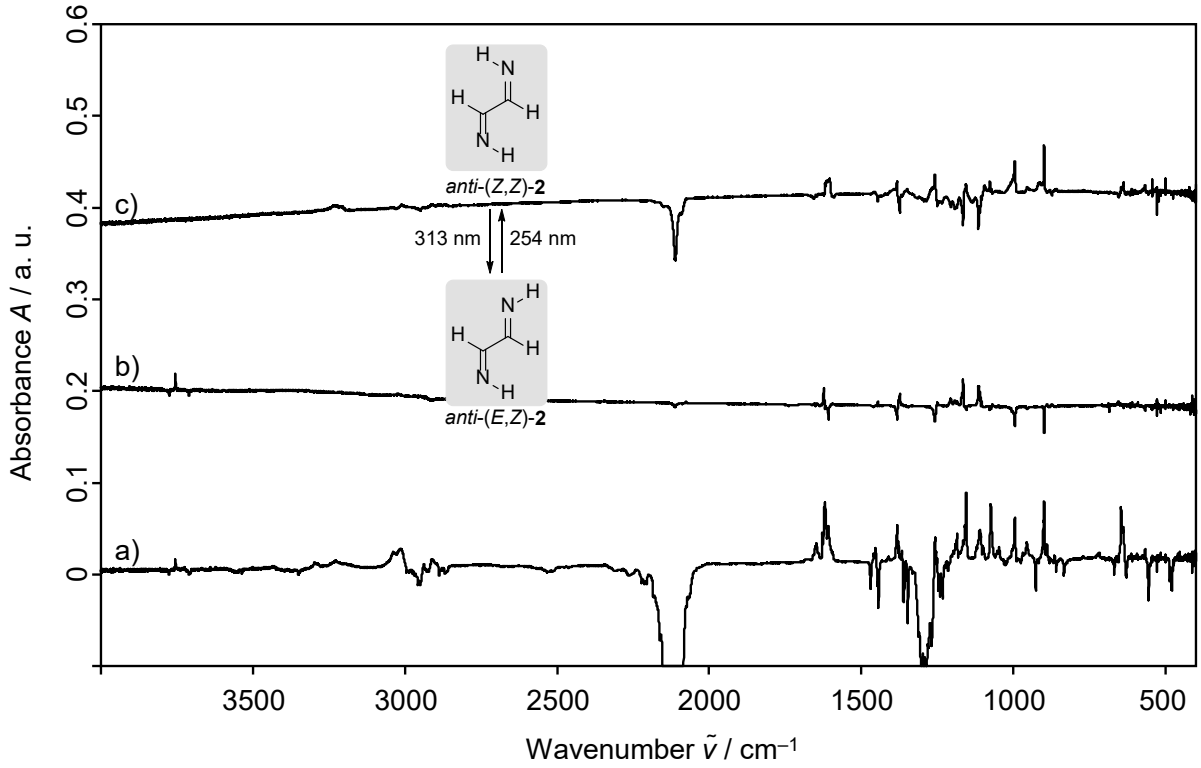

Figure S2: a) Same spectrum as in Figure 1 a); b) Same spectrum as in Figure 1 d); c) IR difference spectrum between the matrix IR spectrum recorded after 1 h irradiation of the matrix with λ = 254 nm (*c.f.* b)) and the spectrum recorded after 70 min irradiation of the matrix with $\lambda > 313$ nm.

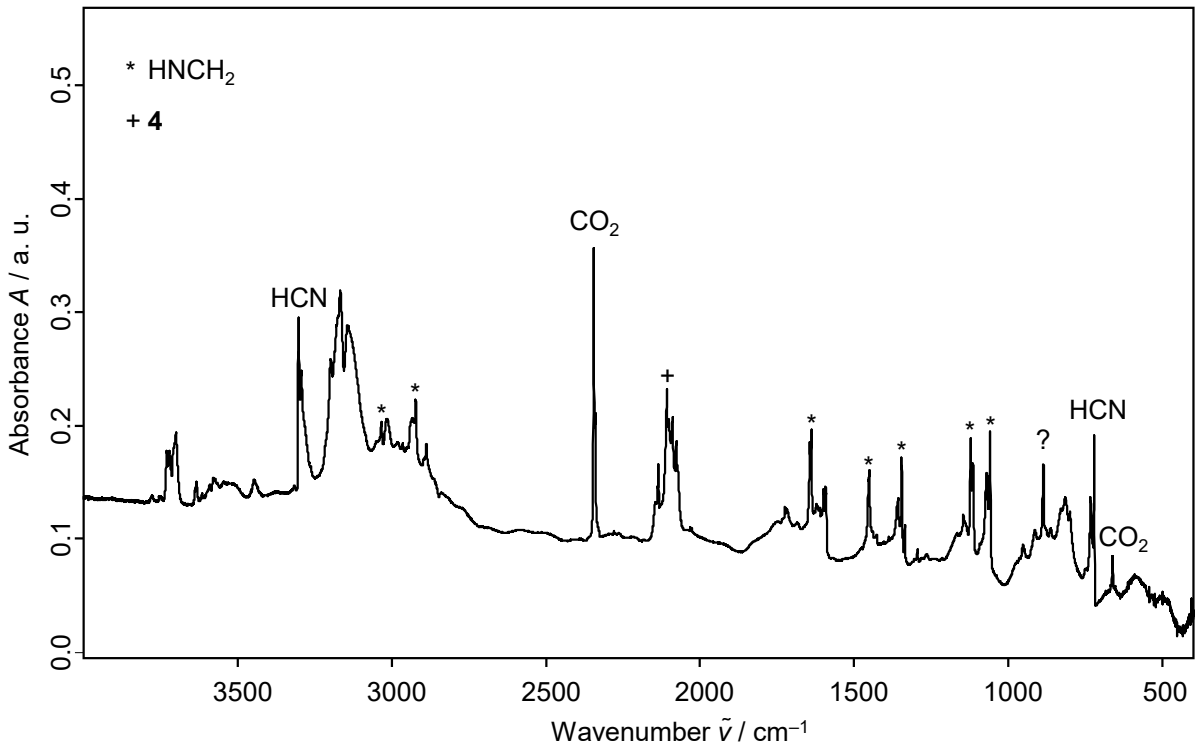

Figure S3: High-vacuum flash pyrolysis (HVFP) spectrum of **4** at 600°C.

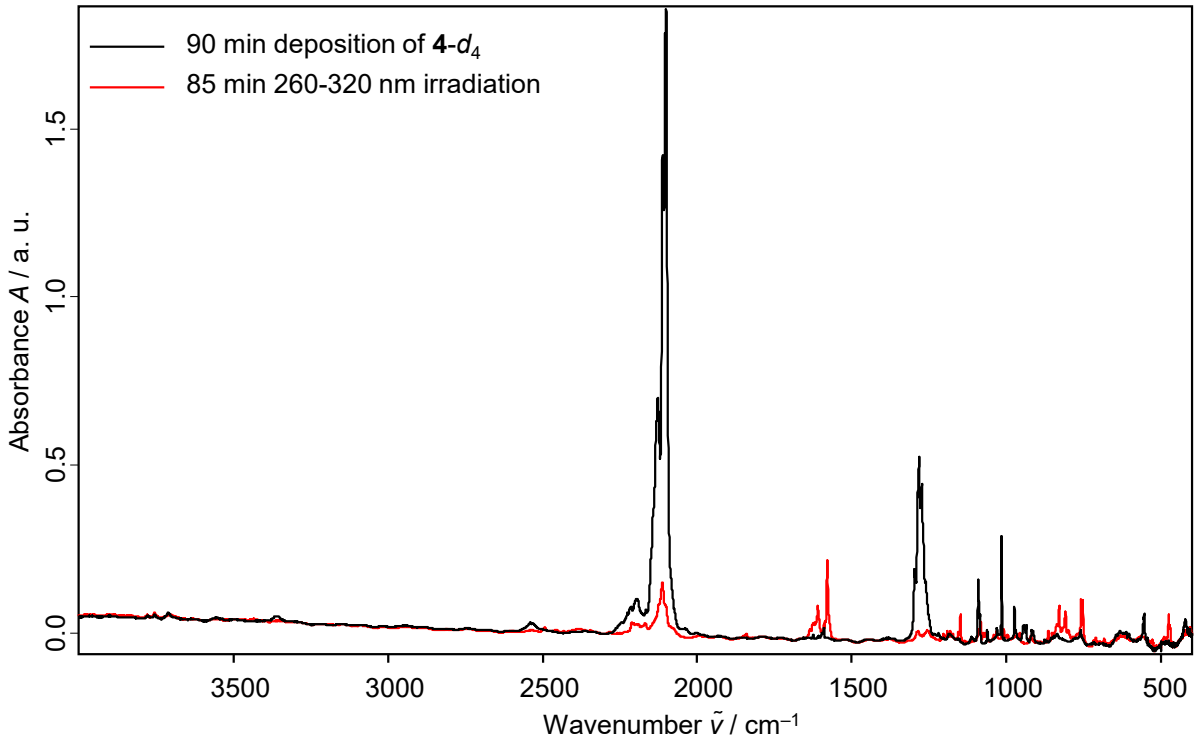

Figure S4: Black: IR-spectrum recorded after 90 min deposition of 1,2-diazidoethane-d_4 (**4**-d_4) at 15 °C isolated in an excess of solid argon at 3 K; Red: Irradiation of the same matrix with UV light (λ = 260 – 320 nm) for 85 min.

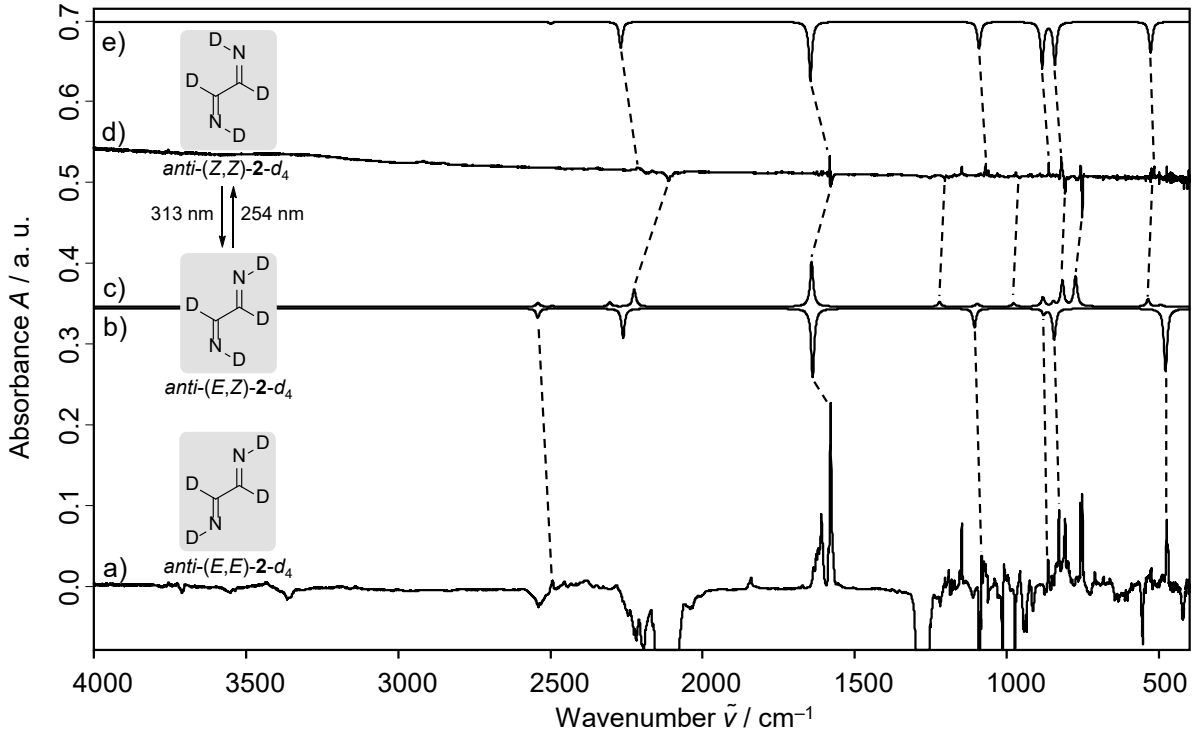

Figure S5: a) IR difference spectrum between the matrix IR spectrum recorded after 90 min deposition of deuterated 1,2-diazidoethane-d_4 (**4**-d_4) and the spectrum recorded after 85 min irradiation of the matrix with UV light (λ = 260 – 320 nm); b) Computed harmonic IR spectrum of *anti*-(*E*,*E*)-**2**-d_4 at the B3LYP/6-311++G(2d,2p) level of theory (unscaled); c) Computed harmonic IR spectrum of *anti*-(*E*,*Z*)-**2**-d_4 at the B3LYP/6-311++G(2d,2p) level of theory (unscaled); c) IR difference spectrum between the matrix IR spectrum recorded after 85 min irradiation of the matrix with UV light (λ = 260 – 320 nm, a) and the spectrum recorded after 2 h irradiation of the matrix with λ = 254 nm; e) Computed harmonic IR spectrum of *anti*-(*Z*,*Z*)-**2**-d_4 at the B3LYP/6-311++G(2d,2p) level of theory (unscaled).

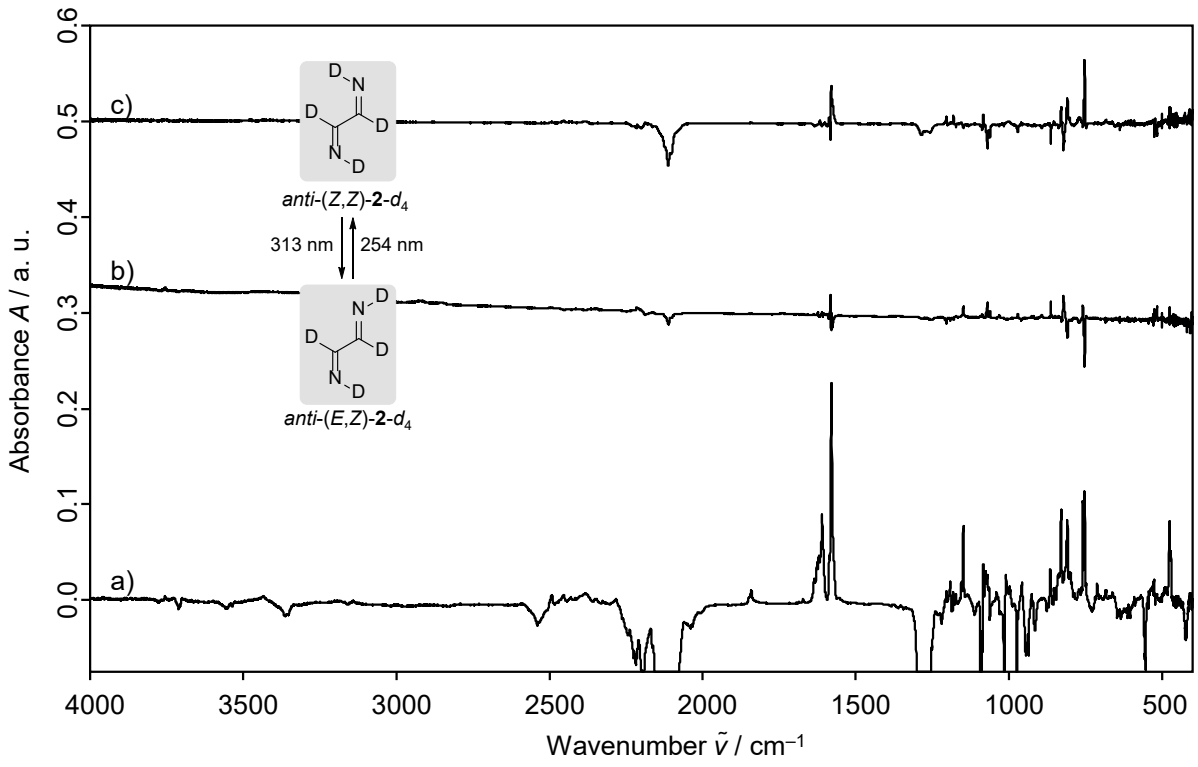

Figure S6: a) Same spectrum as in Figure S4 a); b) Same spectrum as in Figure S4 c); c) IR difference spectrum between the matrix IR spectrum recorded after 2 h irradiation of the matrix with λ = 254 nm (*c.f.* b)) and the spectrum recorded after 70 min irradiation of the matrix with λ = 313 nm.

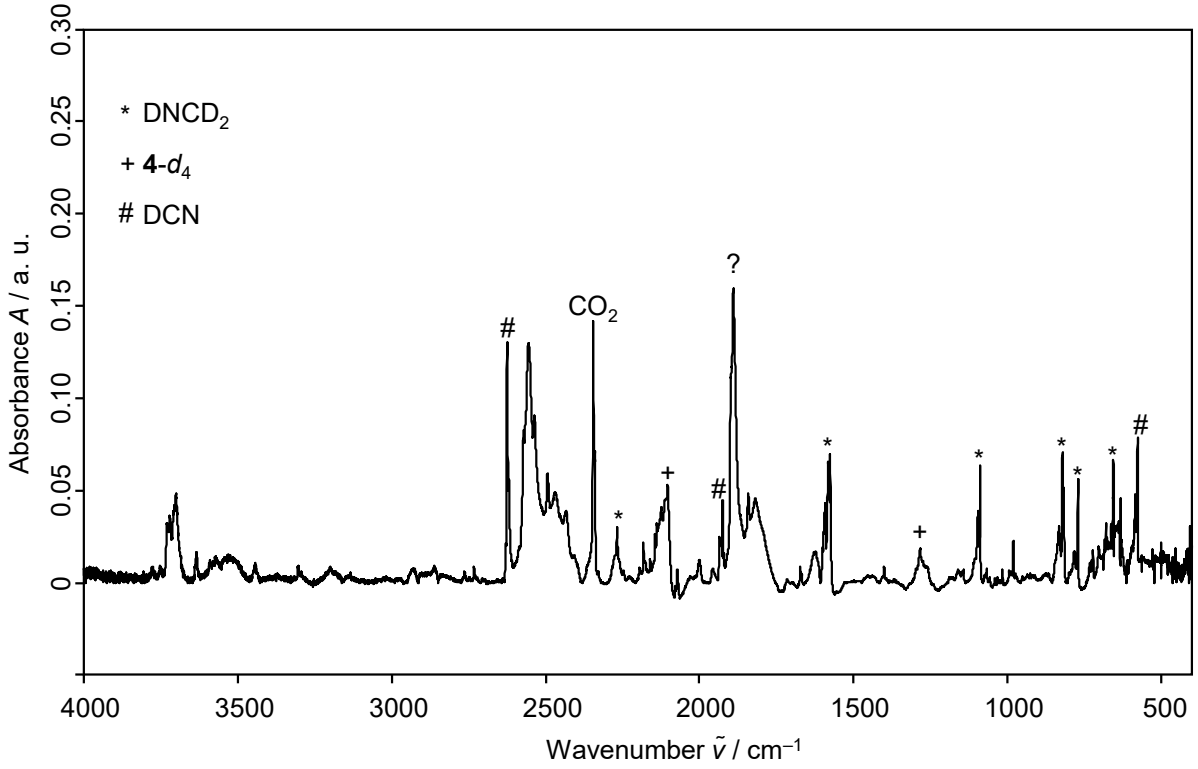

Figure S7: High-vacuum flash pyrolysis (HVFP) spectrum of **4**-d_4 at 600°C.

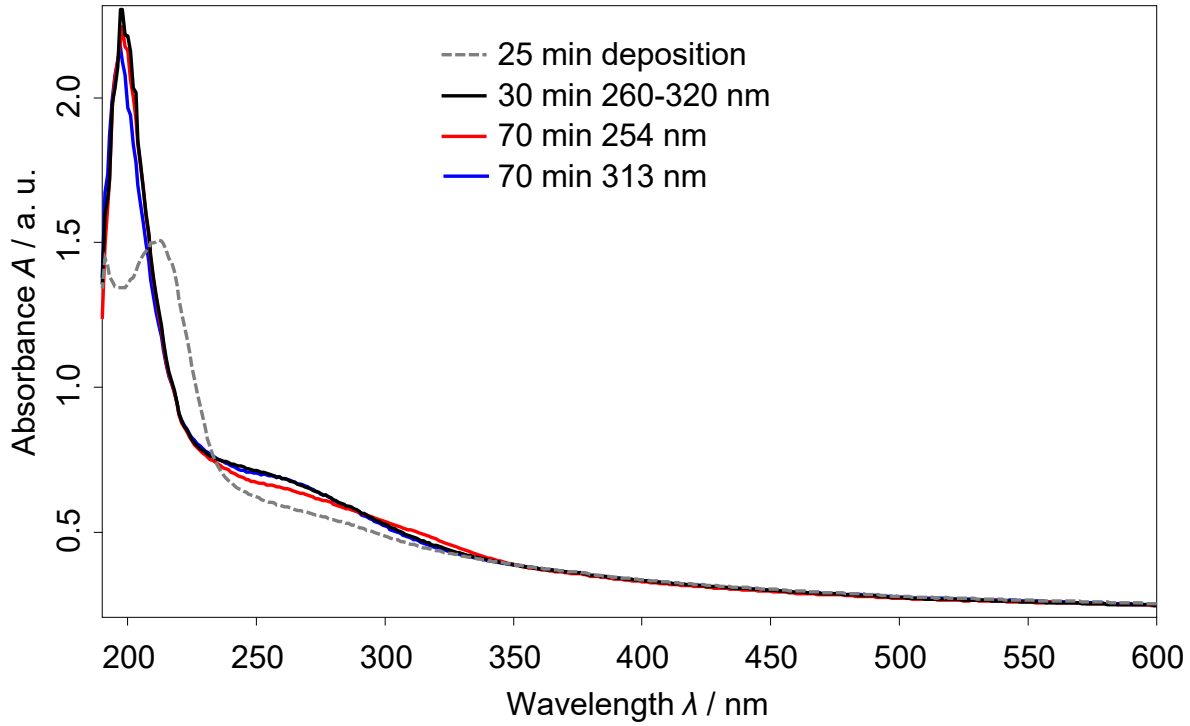

Figure S8: Full range UV/Vis spectra. Note the change in the spectrum after 313 nm irradiation (blue spectrum).

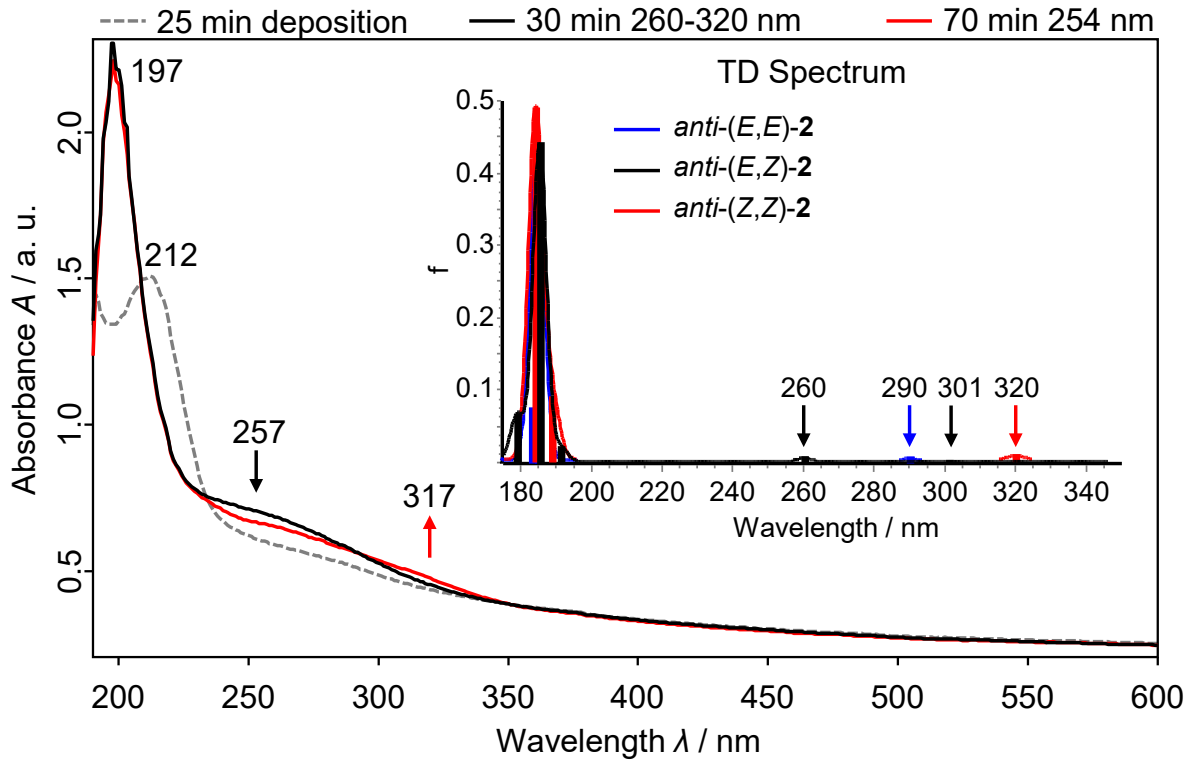

Figure 2 Extension.

IR Spectroscopic Data

Table S1: Comparison of experimental vibrational frequencies of *anti*-(*E*,*E*)-**2** isolated in an argon matrix at 3 K and computed vibrational frequencies at the B3LYP/6-311++G(2d,2p) level of theory (unscaled).

Mode	Sym.	$\tilde{\nu}_{harm.}$ / cm^{-1}	$I_{calc.}$ / km mol^{-1}	$\tilde{\nu}_{exp.}$ / cm^{-1}	I_{rel}
3	A_g	588.3	0.0	-	-
4	A_u	651.3	150.5	645.5	s
5	B_g	920.7	0.0	-	-
6	A_g	996.8	0.0	-	-
7	B_g	1111.6	0.0	-	-
8	A_u	1134.7	7.9	n. o.	n. o.
9	B_u	1181.7	94.1	1155.2	s
10	A_g	1279.6	0.0	-	-
11	B_u	1382.5	51.3	n. o.	n. o.
12	A_g	1427.2	0.0	-	-
13	B_u	1671.4	73.6	1603.5	m
14	A_g	1704.9	0.0	-	-
15	A_g	3058.2	0.0	-	-
16	B_u	3061.0	48.9	3113.6	w
17	B_u	3472.7	8.0	n. o.	n. o.
18	A_g	3473.4	0.0	-	-

rel. experimental intensities (vw = very weak, w = weak, m = middle, s = strong, vs = very strong); n. o. = not observed.

Table S2: Comparison of experimental vibrational frequencies of *anti*-(*E*,*Z*)-**2** isolated in an argon matrix at 3 K and computed vibrational frequencies at the B3LYP/6-311++G(2d,2p) level of theory (unscaled).

Mode	Sym.	$\tilde{\nu}_{harm.}$ / cm^{-1}	$I_{calc.}$ / km mol^{-1}	$\tilde{\nu}_{exp.}$ / cm^{-1}	I_{rel}
3	A'	576.3	9.3	n. o.	n. o.
4	A"	653.7	8.8	n. o.	n. o.
5	A"	928.1	50.7	898.7	s
6	A'	1005.0	72.0	995.7	s
7	A"	1108.2	29.7	1077.2	w
8	A'	1144.5	32.4	1096.0	w
9	A'	1194.3	3.4	n. o.	n. o.
10	A'	1288.0	65.1	1258.3	m
11	A'	1396.5	3.2	n. o.	n. o.
12	A'	1418.1	38.1	1382.5	m
13	A'	1669.4	70.0	1621.4	m
14	A'	1697.3	1.4	n. o.	n. o.
15	A'	3009.3	42.7	2914.0	vw
16	A'	3115.2	10.6	n. o.	n. o.
17	A'	3409.5	3.4	n. o.	n. o.
18	A'	3468.9	4.2	n. o.	n. o.

rel. experimental intensities (vw = very weak, w = weak, m = middle, s = strong, vs = very strong); n. o. = not observed.

Table S3: Comparison of experimental vibrational frequencies of *anti*-(*Z*,*Z*)-**2** isolated in an argon matrix at 3 K and computed vibrational frequencies at the B3LYP/6-311++G(2d,2p) level of theory (unscaled).

Mode	Sym.	$\tilde{\nu}_{harm.}$ / cm^{-1}	$I_{calc.}$ / km mol^{-1}	$\tilde{\nu}_{exp.}$ / cm^{-1}	I_{rel}
3	A_g	564.0	0.0	-	-
4	A_u	663.8	49.8	654.1	vw
5	B_g	936.7	0.0	-	-
6	A_g	1021.4	0.0	-	-
7	B_g	1111.5	0.0	-	-
8	A_u	1149.3	108.9	1115.0	m
9	B_u	1200.7	135.1	1165.3	s
10	A_g	1297.5	0.0	-	-
11	B_u	1409.8	60.7	1373.3	m
12	A_g	1416.0	0.0	-	-
13	B_u	1667.9	68.6	1618.5	m
14	A_g	1691.1	0.0	-	-
15	A_g	3068.3	0.0	-	-
16	B_u	3072.5	44.4	3021.3	vw
17	B_u	3415.5	4.2	n. o.	n. o.
18	A_g	3418.9	0.0	-	-

rel. experimental intensities (vw = very weak, w = weak, m = middle, s = strong, vs = very strong); n. o. = not observed.

Table S4: Comparison of experimental vibrational frequencies of deuterated *anti*-(*E*,*E*)-**2**-d_4 isolated in an argon matrix at 3 K and computed vibrational frequencies at the B3LYP/6-311++G(2d,2p) level of theory (unscaled).

Mode	Sym.	$\tilde{\nu}_{harm.}$ / cm^{-1}	$I_{calc.}$ / km mol^{-1}	$\tilde{\nu}_{exp.}$ / cm^{-1}	I_{rel}
3	A_u	478.9	79.1	475.5	s
4	A_g	562.5	0.0	-	-
5	B_g	737.8	0.0	-	-
6	A_g	802.7	0.0	-	-
7	B_u	844.8	39.4	828.3	s
8	A_u	878.9	7.3	865.0	vw
9	B_g	897.9	0.0	-	-
10	A_g	960.2	0.0	-	-
11	B_u	1106.5	23.5	1083.5	w
12	A_g	1256.8	0.0	-	-
13	B_u	1637.9	86.2	1578.4	m
14	A_g	1662.6	0.0	-	-
15	B_u	2260.8	37.0	2212.0	w
16	A_g	2264.5	0.0	-	-
17	A_g	2540.5	0.0	-	-
18	B_u	2541.4	11.8	2492.5	w

rel. experimental intensities (vw = very weak, w = weak, m = middle, s = strong, vs = very strong); n. o. = not observed.

Table S5: Comparison of experimental vibrational frequencies of deuterated *anti*-(*E*,*Z*)-**2**-d_4 isolated in an argon matrix at 3 K and computed vibrational frequencies at the B3LYP/6-311++G(2d,2p) level of theory (unscaled).

Mode	Sym.	$\tilde{\nu}_{harm.}$ / cm^{-1}	$I_{calc.}$ / km mol^{-1}	$\tilde{\nu}_{exp.}$ / cm^{-1}	I_{rel}
3	A"	495.2	3.9	n. o.	n. o.
4	A'	536.4	13.5	527.7	vw
5	A"	774.5	54.3	752.7	s
6	A'	817.9	45.6	808.4	m
7	A"	847.4	7.6	n. o.	n. o.
8	A'	881.5	17.1	n. o.	n. o.
9	A"	889.2	0.1	n. o.	n. o.
10	A'	977.8	6.1	958.8	vw
11	A'	1097.9	5.7	n. o.	n. o.
12	A'	1221.3	8.2	1203.3	vw
13	A'	1641.4	80.7	1580.4	s
14	A'	1663.4	0.3	n. o.	n. o.
15	A'	2224.2	31.5	2187.3	vw
16	A'	2304.4	8.4	n. o.	n. o.
17	A'	2493.6	1.4	n. o.	n. o.
18	A'	2540.7	6.3	n. o.	n. o.

rel. experimental intensities (vw = very weak, w = weak, m = middle, s = strong, vs = very strong); n. o. = not observed.

Table S6: Comparison of experimental vibrational frequencies of deuterated *anti*-(*Z*,*Z*)-**2** isolated in an argon matrix at 3 K and computed vibrational frequencies at the B3LYP/6-311++G(2d,2p) level of theory (unscaled).

Mode	Sym.	$\tilde{\nu}_{harm.}$ / cm^{-1}	$I_{calc.}$ / km mol^{-1}	$\tilde{\nu}_{exp.}$ / cm^{-1}	I_{rel}
3	A_g	510.8	0.0	-	-
4	A_u	527.9	39.7	516.6	vw
5	B_g	792.2	0.0	-	-
6	A_u	842.6	54.9	821.8	m
7	B_g	866.3	0.0	-	-
8	A_g	869.4	0.0	-	-
9	B_u	884.3	59.7	862.8	w
10	A_g	1000.6	0.0	-	-
11	B_u	1091.5	35.5	1070.2	w
12	A_g	1183.5	0.0	-	-
13	B_u	1645.4	77.0	1582.2	s
14	A_g	1663.6	0.0	-	-
15	B_u	2268.6	34.1	2213.5	vw
16	A_g	2271.1	0.0	-	-
17	B_u	2499.1	2.9	n. o.	n. o.
18	A_g	2500.0	0.0	-	-

rel. experimental intensities (vw = very weak, w = weak, m = middle, s = strong, vs = very strong); n. o. = not observed.

UV/Vis Spectroscopic Data

Table S7: TD-DFT B3LYP/6-311++G(2d,2p) computed vertical excitation energies of *anti*-(*E*,*E*)-**2** and comparison with the recorded UV/Vis photolysis spectrum.

excitation energy λ / nm	oscillator strength (*f*)	$\lambda_{exp.}$ / nm	transition
290.0	0.0017	297	HOMO – LUMO
184.7	0.403	197	HOMO–2 – LUMO HOMO–1 – LUMO+1
183.0	0.0698	out of range	HOMO–2 – LUMO HOMO–1 – LUMO+1 HOMO – LUMO+2

Table S8: TD-DFT B3LYP/6-311++G(2d,2p) computed vertical excitation energies of *anti*-(*E*,*Z*)-**2** and comparison with the recorded UV/Vis photolysis spectrum.

excitation energy λ / nm	oscillator strength (*f*)	$\lambda_{exp.}$ / nm	transition
301.1	0.0005	n. o.	HOMO – LUMO
260.1	0.0046	257	HOMO–1 – LUMO
191.0	0.0198	197	HOMO–2 – LUMO HOMO–1 – LUMO+1 HOMO – LUMO+1
185.2	0.439	out of range	HOMO–2 – LUMO HOMO – LUMO+1

Table S9: TD-DFT B3LYP/6-311++G(2d,2p) computed vertical excitation energies of *anti*-(*Z*,*Z*)-**2** and comparison with the recorded UV/Vis photolysis spectrum.

excitation energy λ / nm	oscillator strength (*f*)	$\lambda_{exp.}$ / nm	transition
320.1	0.0051	320	HOMO – LUMO
188.9	0.0838	197	HOMO–1 – LUMO HOMO – LUMO+1
184.2	0.4833	out of range	HOMO–1 – LUMO HOMO – LUMO+1

NMR and ESI-MS Spectra

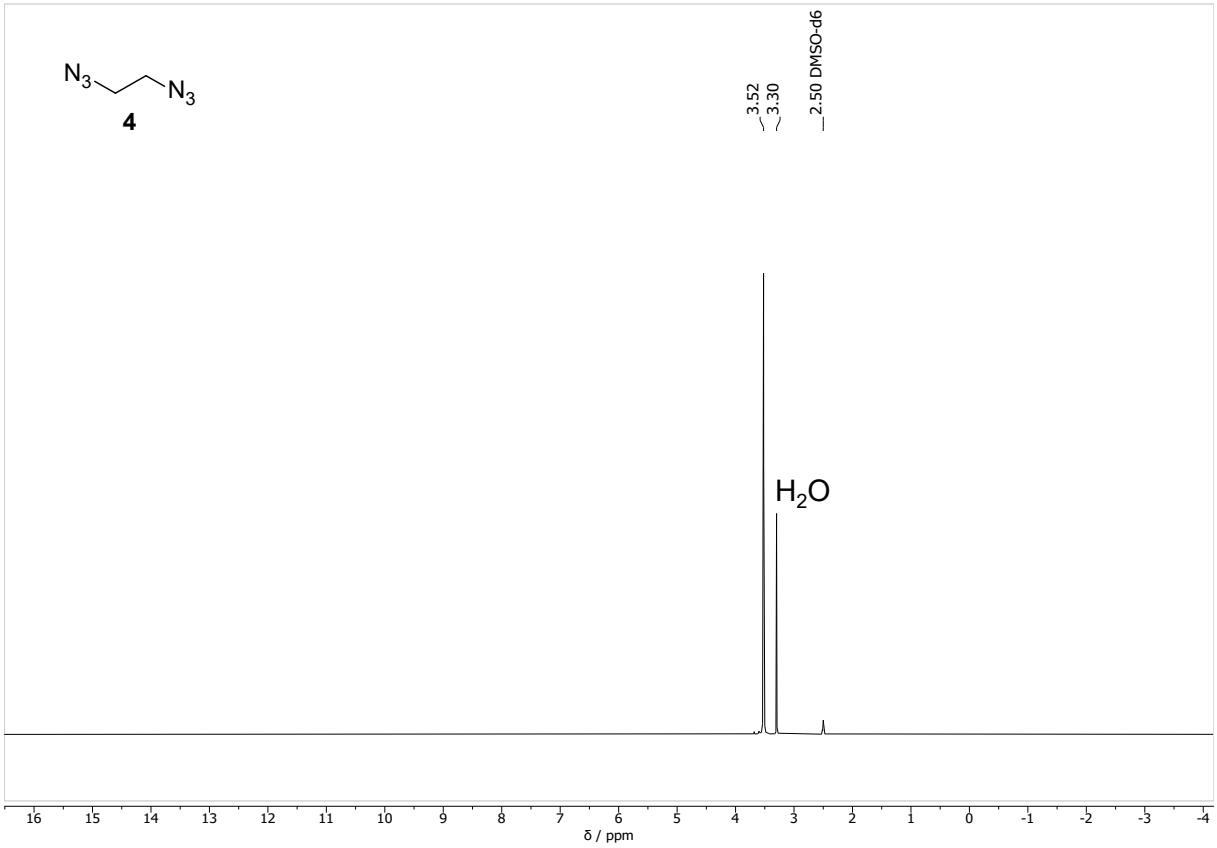

Figure S9: ^{1}H NMR (300 MHz, DMSO-d_6) spectrum of 1,2-diazidoethane (**4**).

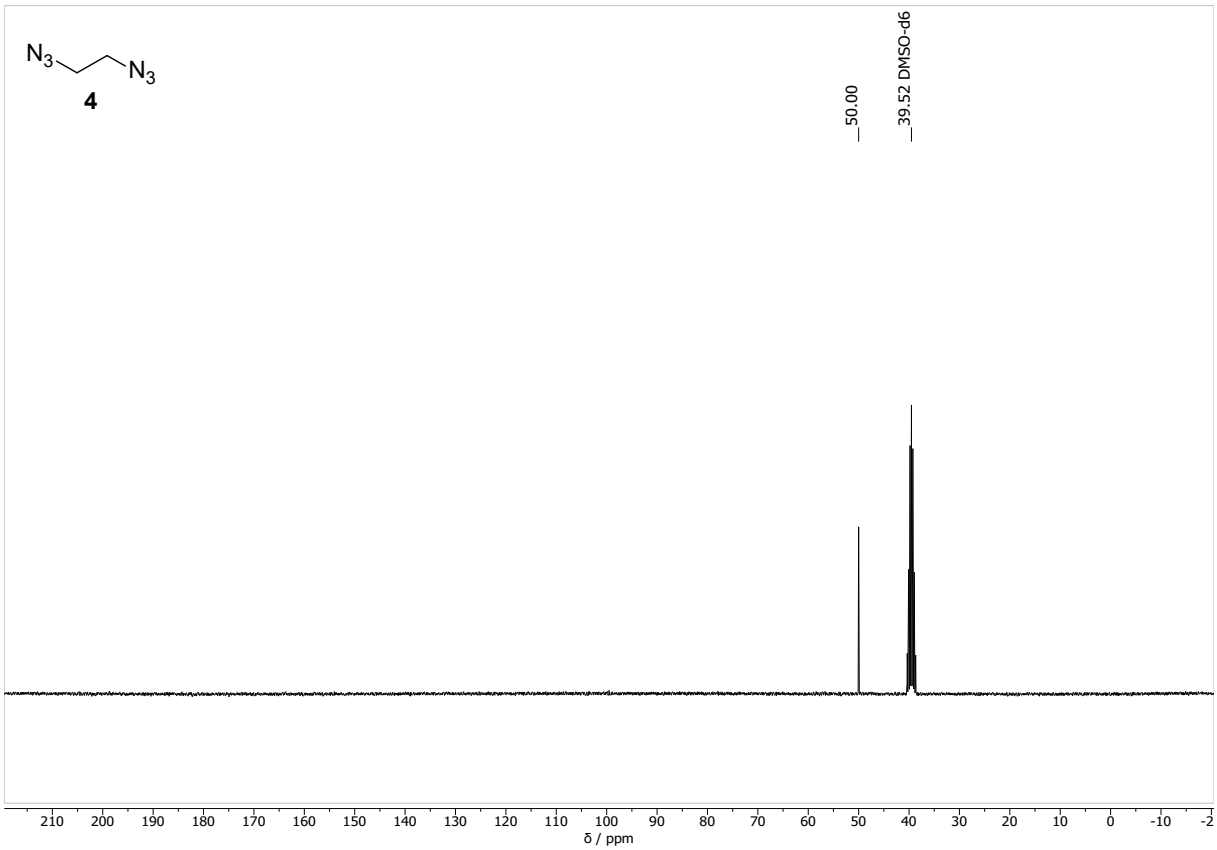

Figure S10: ^{13}C NMR (76 MHz, DMSO-d_6) spectrum of 1,2-diazidoethane (**4**).

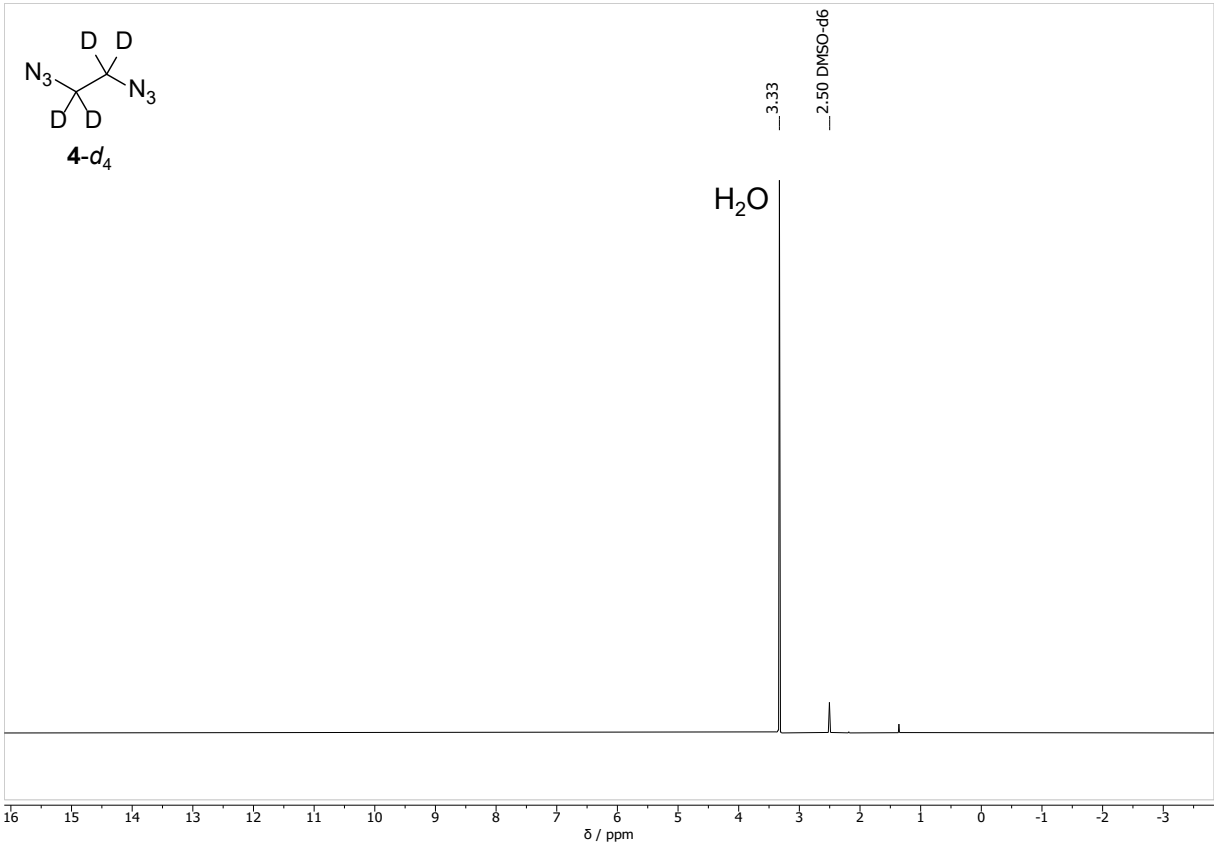

Figure S11: ^{1}H NMR (300 MHz, DMSO-d_6) spectrum of deuterated 1,2-diazidoethane-d_4 (**4**-d_4).

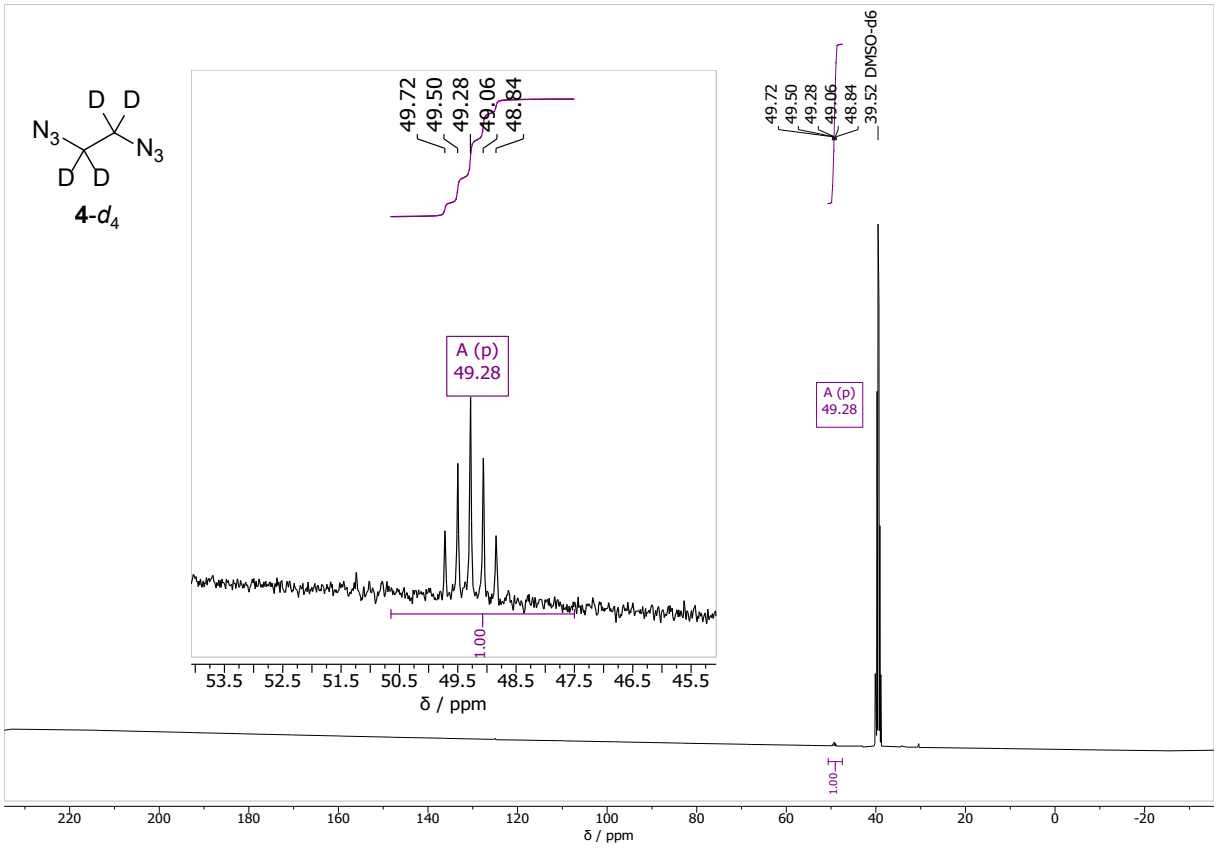

Figure S12: ^{13}C{^{1}H} NMR (101 MHz, DMSO-d_6) spectrum of deuterated 1,2-diazidoethane-d_4 (**4**-d_4).

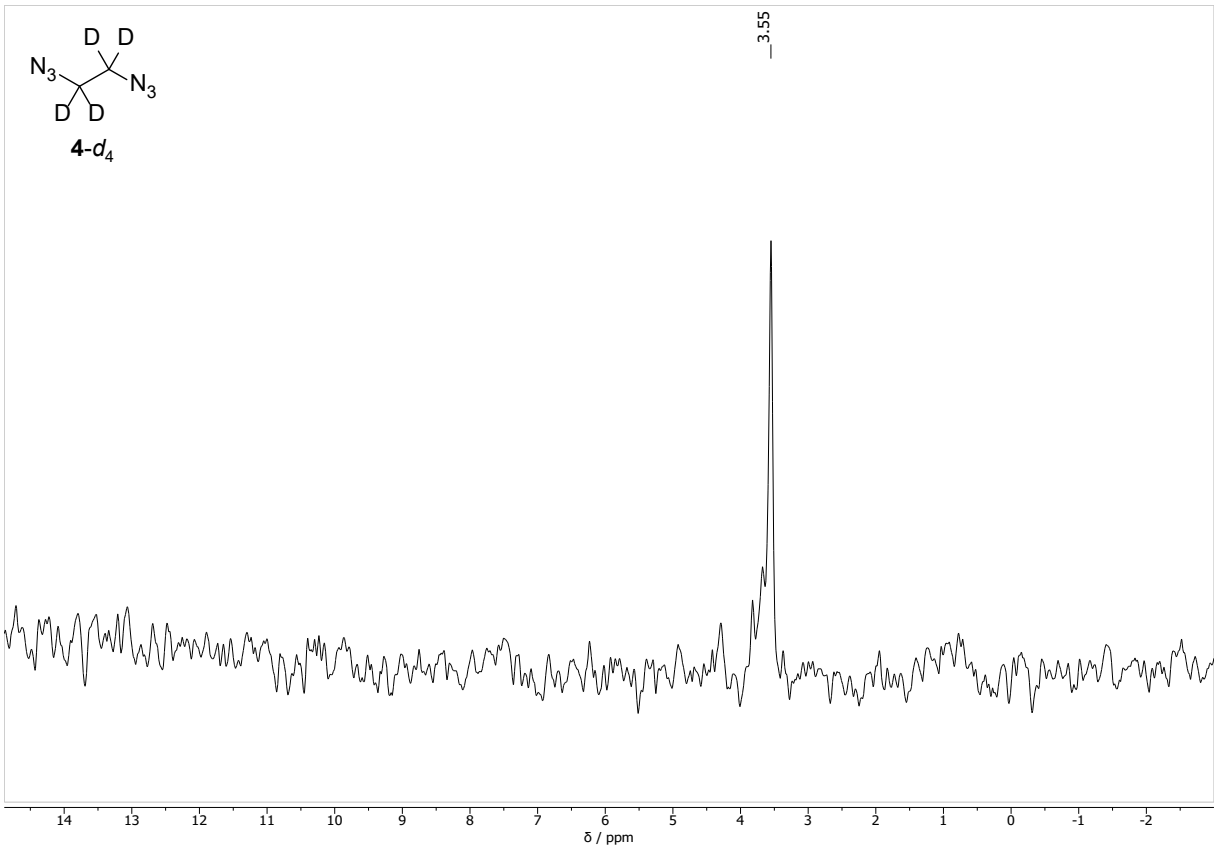

Figure S13: ^{2}D NMR (62 MHz, DMSO) spectrum of deuterated 1,2-diazidoethane-d_4 (**4**-d_4).

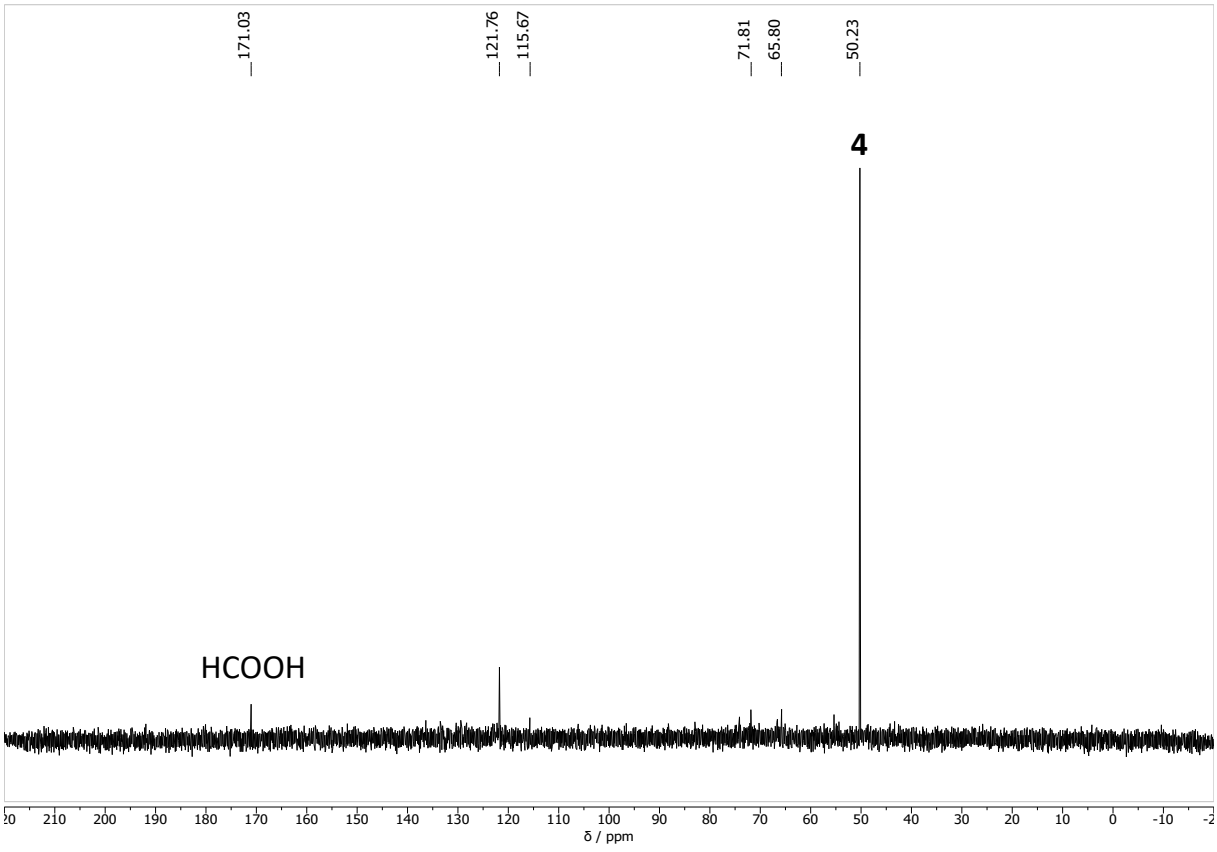

Figure S14: ^{13}C NMR (101 MHz, D_2O) spectrum of the experiment shown in Figure 4.

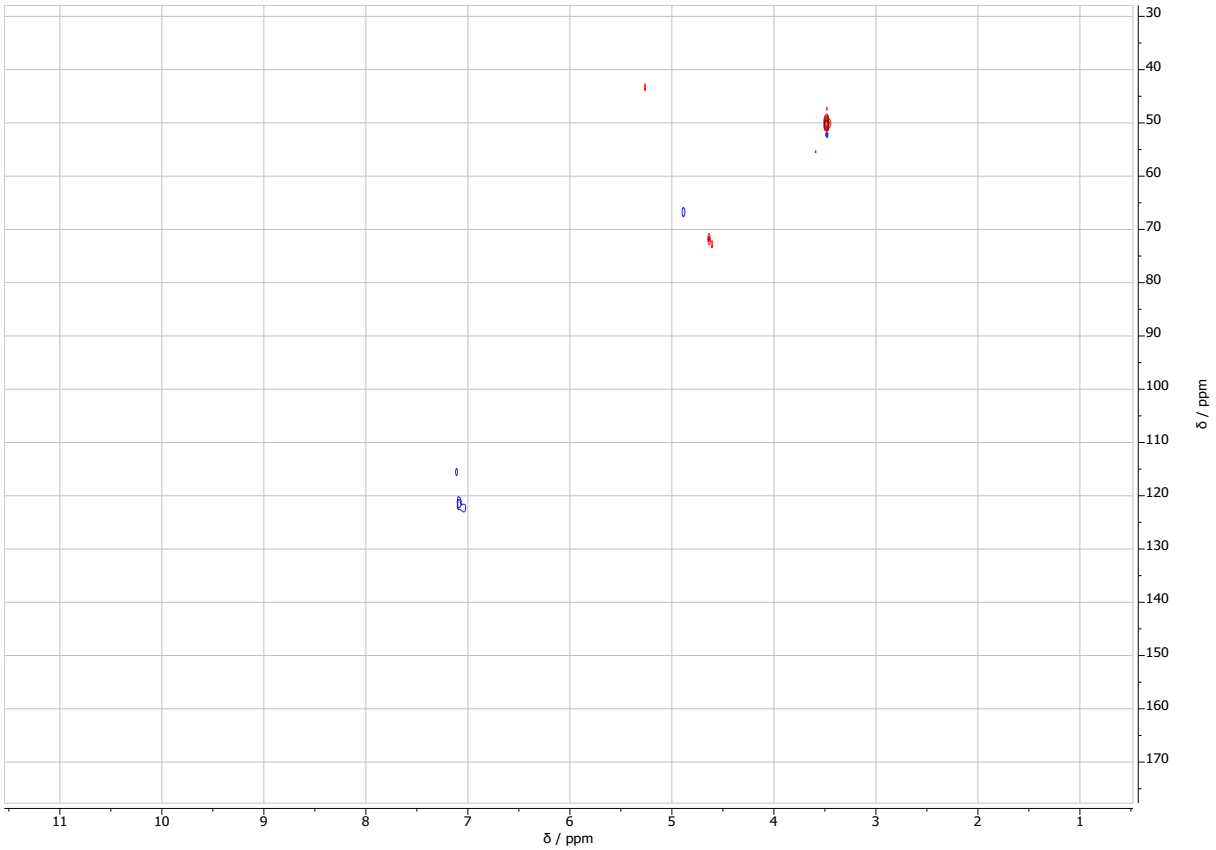

Figure S15: HSQC 2D NMR spectrum of the experiment shown in Figure 4.

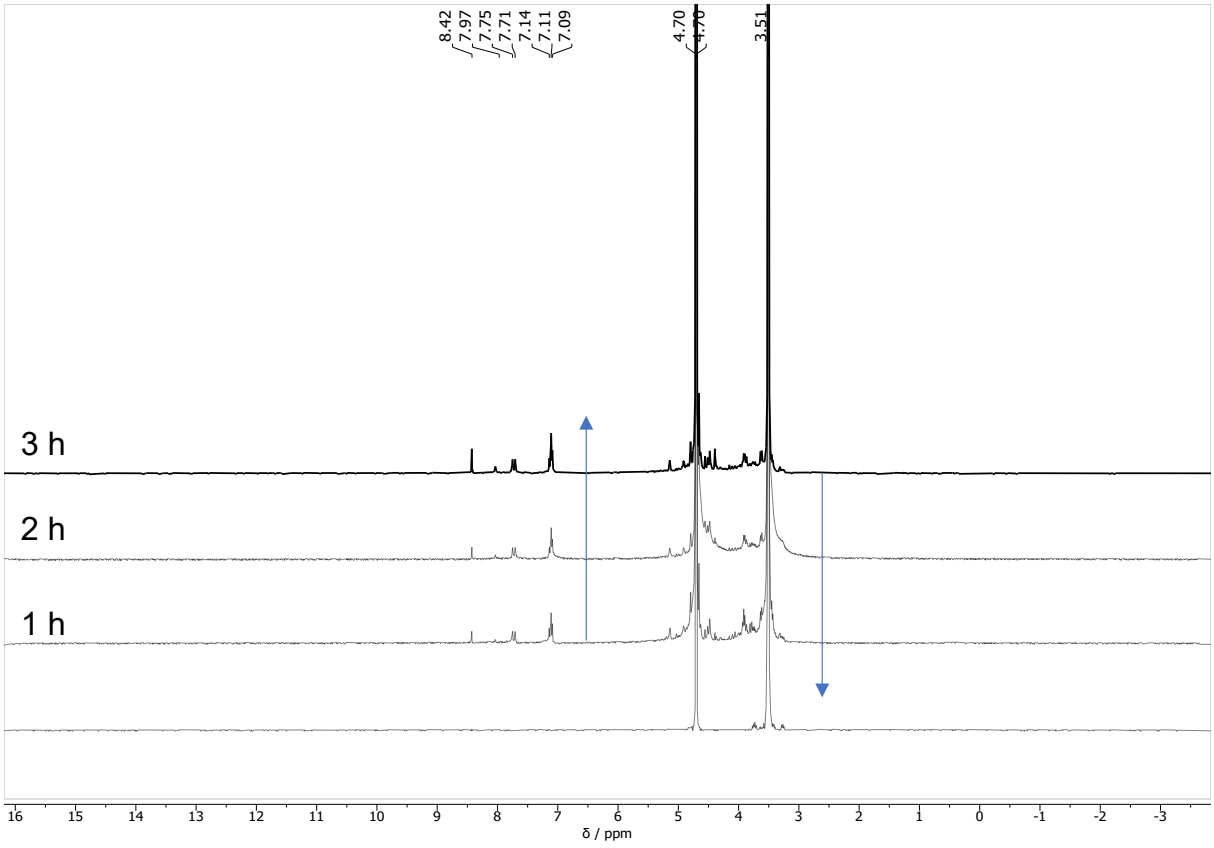

Figure S16: ^{1}H NMR (400 MHz, D_2O) spectra measured during the irradiation of 1,2-diazidoethane (**4**) in D_2O with 260-320 nm over a time period of 3 h.

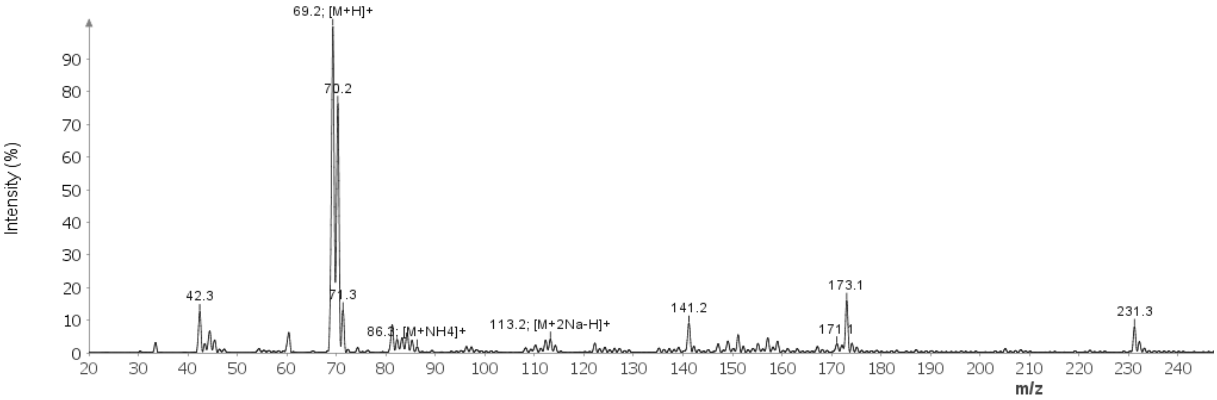

Figure S17: ESI-MS spectrum of the NMR solution depicted in Figure 4.

GC-MS Data

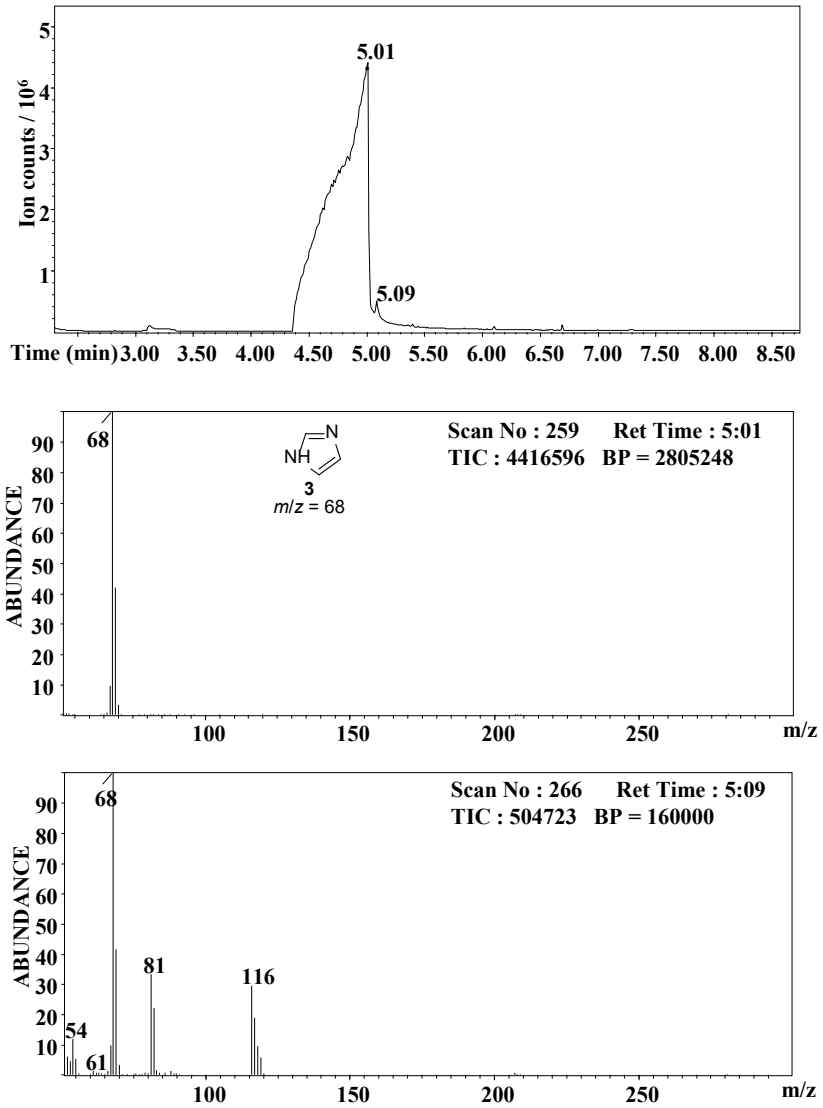

Figure S18: GC-MS reference chromatograms of imidazole (**3**), which was previously dissolved in D_2O and the solvent evaporated at room temperature overnight. The single peak at 5.09 min cannot be unambiguously assigned.

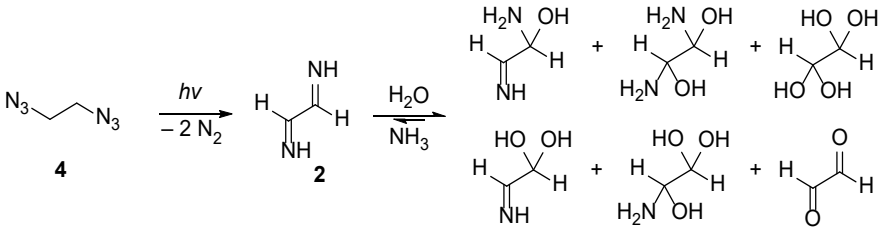

Scheme S1: Possible equilibrium structures of 1,2-diimonoethane (**2**) in aqueous solution.

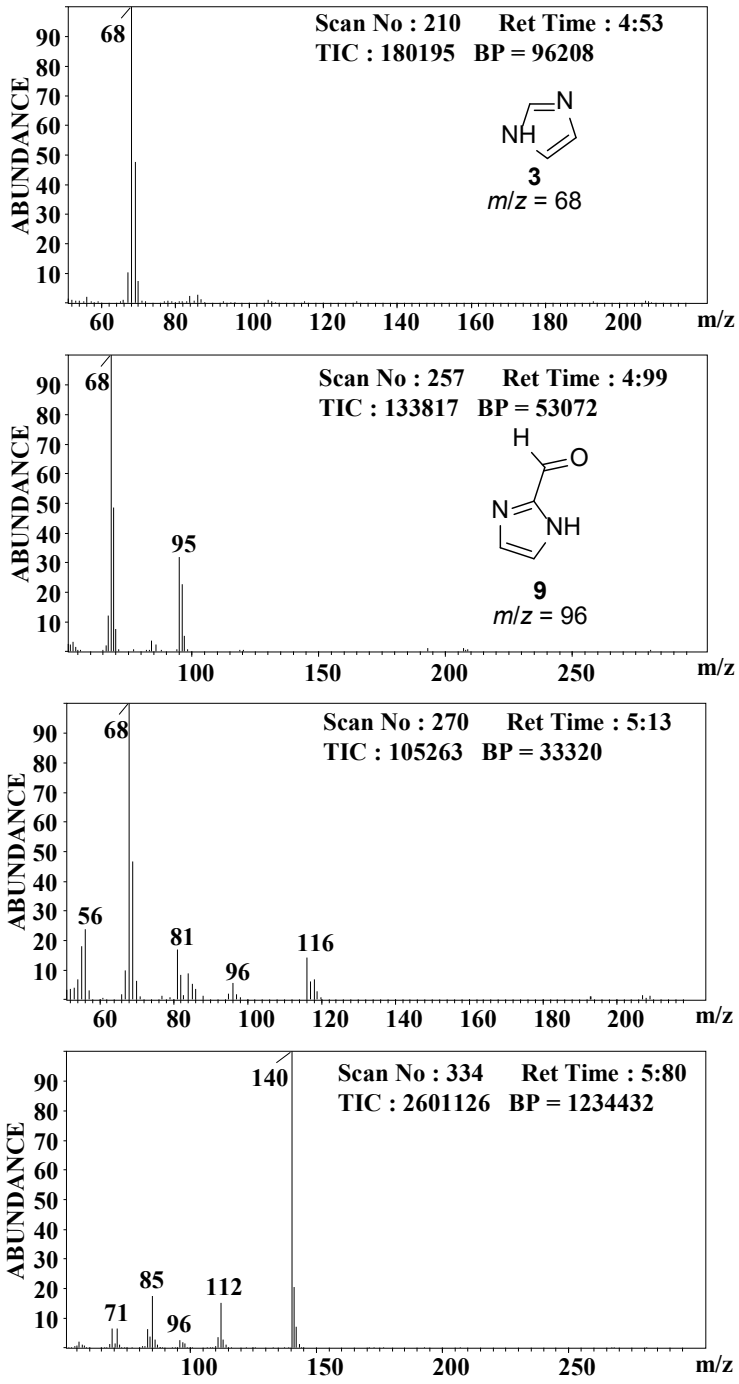

Figure S19: MS spectra of the chromatogram depicted in Figure 4. The peak at 5:80 min is tentatively assigned to **11**.

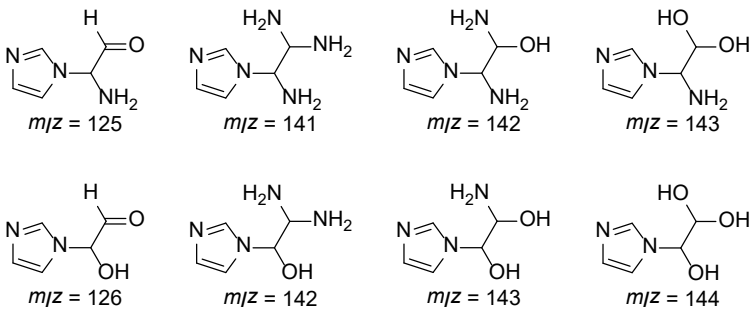

Scheme S2: Possible hydrolyzed *N*-glyoxal substituted imidazole species.

Potential Energy Surfaces and Electronic Energies for Selected Structures

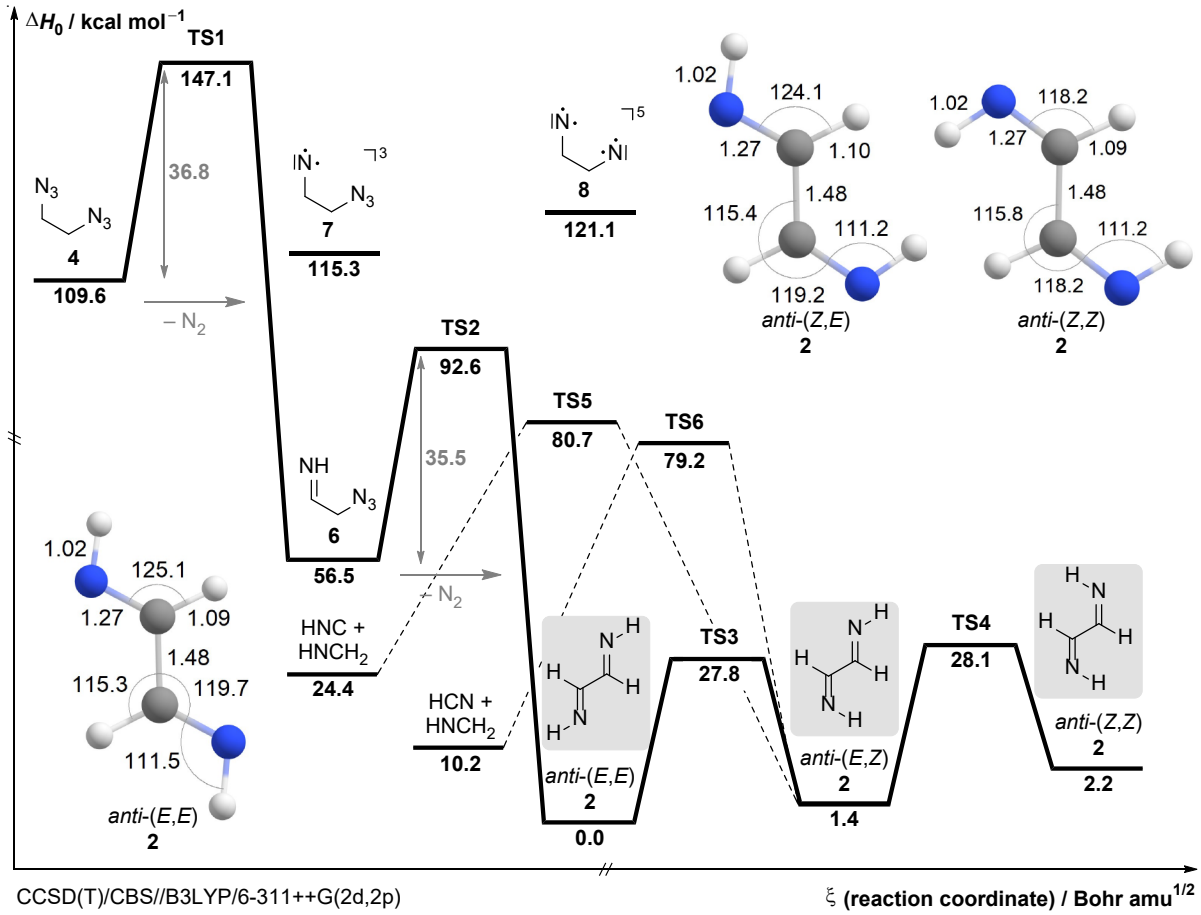

Figure 3 Extension.

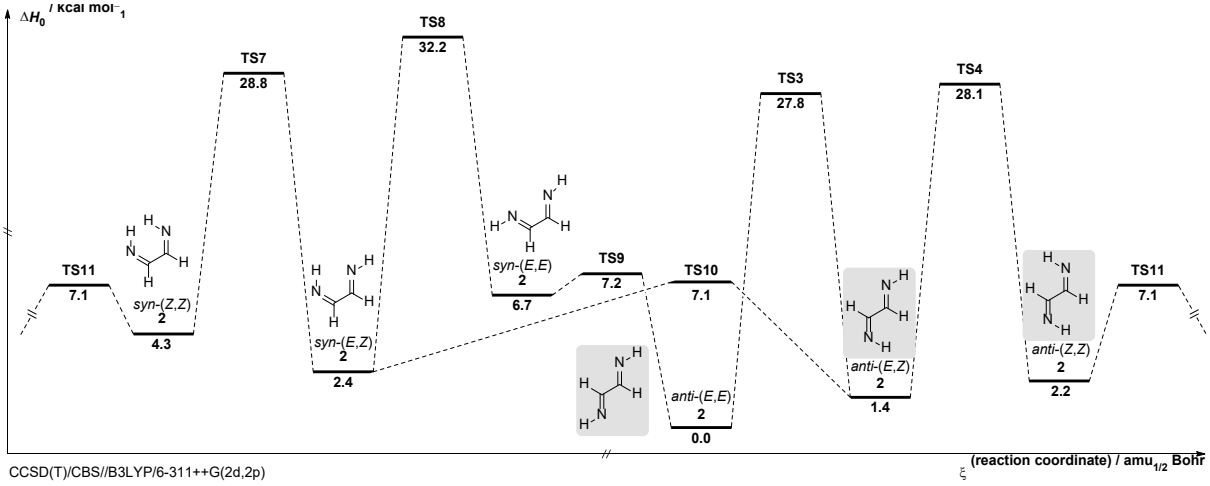

Figure S20: Rotational energy profile of 1,2-diiminoethane (**2**). Note that the profile is a circle with **TS11** connecting *syn*-(*Z*,*Z*)-**2** on the left and *anti*-(*Z*,*Z*)-**2** on the right.

All cartesian coordinates can be found in the uploaded .xyz files.

Table S10: B3LYP/6-311++G(2d,2p) optimized structures, electronic energies (in Hartree), zero-point vibrational energies (ZPVEs in Hartree), CCSD(T)/CBS energies (in Hartree) and relative energies of all structures depicted in Figure 4 and Figure S20.

Compound	E	ZPVE	CCSD(T)/CBS	ΔE(B3LYP) / kcal mol^{-1}	ΔE(CCSD(T)) / kcal mol^{-1}
1.2-diazidoethane (**4**)	–407.116881	0.082674	–406.538633	**104.18**	**109.64**
1-azido-2-nitrenoethane (**7**)	–297.539018	0.069966	–297.099644	**108.71**	**115.27**
1-azido-2-iminoethane (**6**)	–297.629418	0.072647	–297.195909	**53.67**	**56.55**
1,2-dinitrenoethane (**8**)	–187.959376	0.057363	–187.660384	**114.43**	**121.14**
anti-(*E*,*E*)-**2**	–188.147310	0.062946	–187.859014	**0.00**	**0.00**
anti-(*Z*,*E*)-**2**	–188.144729	0.062835	–187.856631	**1.55**	**1.43**
anti-(*Z*,*Z*)-**2**	–188.143307	0.062827	–187.855367	**2.44**	**2.21**
syn-(*E*,*E*)-**2**	–188.135735	0.062461	–187.847914	**6.96**	**6.66**
syn-(*Z*,*E*)-**2**	–188.139060	0.062647	–187.855031	**4.99**	**2.31**
syn-(*Z*,*Z*)-**2**	–188.142181	0.062862	–187.851914	**3.17**	**4.40**
TS1	–407.048137	0.075913	–406.472140	**143.08**	**147.12**
TS2	–297.563650	0.066090	–297.131824	**90.82**	**92.65**
TS3	–188.102655	0.059943	–187.811771	**26.14**	**27.76**
TS4	–188.101791	0.059838	–187.811088	**26.61**	**28.12**
TS5	–188.019692	0.055702	–187.723242	**75.54**	**80.65**
TS6	–188.007232	0.055615	–187.725464	**83.30**	**79.20**
TS7	–188.099780	0.059898	–187.810144	**27.91**	**28.75**
TS8	–188.094690	0.059529	–187.804229	**30.87**	**32.23**
TS9	–188.134030	0.061989	–187.846518	**7.73**	**7.24**
TS10	–188.134453	0.062107	–187.846893	**7.54**	**7.08**
TS11	–188.134569	0.062221	–187.847044	**7.54**	**7.06**
HCN (+ **5**)	–93.456797	0.016259	–93.317174	**10.66**	**10.25**
HNC(+ **5**)	–93.434009	0.015327	–93.293643	**24.38**	**24.43**
Formaldimine (**5**)	–94.666690	0.039854	–94.518679		
N_2	–109.563481	0.005547	–109.422855		

Table S11: B3LYP/6-311++G(2d,2p) optimized conformers and relative energies of 1,2-diazidoethane (**4**) based on a conformational search using CREST.

Conformer	E	ZPVE	ΔE / kcal mol^{-1}
1	–407.116114	0.082783	**0.00**
2	–407.116145	0.082776	**–0.02**
3	–407.116065	0.082779	**0.03**
4	–407.114849	0.082746	**0.77**
5	–407.116882	0.082672	**–0.55**
6	–407.117310	0.082693	**–0.81**
7	–407.116427	0.082585	**–0.32**
8	–407.115443	0.082594	**0.30**
9	–407.117048	0.082369	**–0.85**

Table S12: B3LYP/6-311++G(2d,2p) optimized conformers and relative energies of 1-azido-2-iminoethane (**6**) based on a conformational search using CREST.

Conformer	E	ZPVE	ΔE / kcal mol^{-1}
1	–297.628719	0.072588	**0.00**
2	–297.629833	0.072532	–**0.73**
3	–297.626302	0.072498	**1.46**
4	–297.627042	0.072625	**1.08**
5	–297.625520	0.072123	**1.72**
6	–297.629101	0.072251	–**0.45**
7	–297.629418	0.072647	–**0.40**
8	–297.628420	0.072483	**0.12**
9	–297.626525	0.072211	**1.14**

References

(1) Whittle, E.; Dows, D. A.; Pimentel, G. C. *J. Chem. Phys.* **1954**, *22*, 1943-1943.
(2) Gaussian 16 Rev. C.01; Frisch, M. J.; Trucks, G. W.; Schlegel, H. B.; Scuseria, G. E.; Robb, M. A.; Cheeseman, J. R.; Scalmani, G.; Barone, V.; Petersson, G. A.; Nakatsuji, H.; Li, X.; Caricato, M.; Marenich, A. V.; Bloino, J.; Janesko, B. G.; Gomperts, R.; Mennucci, B.; Hratchian, H. P.; Ortiz, J. V.; Izmaylov, A. F.; Sonnenberg, J. L.; Williams; Ding, F.; Lipparini, F.; Egidi, F.; Goings, J.; Peng, B.; Petrone, A.; Henderson, T.; Ranasinghe, D.; Zakrzewski, V. G.; Gao, J.; Rega, N.; Zheng, G.; Liang, W.; Hada, M.; Ehara, M.; Toyota, K.; Fukuda, R.; Hasegawa, J.; Ishida, M.; Nakajima, T.; Honda, Y.; Kitao, O.; Nakai, H.; Vreven, T.; Throssell, K.; Montgomery Jr., J. A.; Peralta, J. E.; Ogliaro, F.; Bearpark, M. J.; Heyd, J. J.; Brothers, E. N.; Kudin, K. N.; Staroverov, V. N.; Keith, T. A.; Kobayashi, R.; Normand, J.; Raghavachari, K.; Rendell, A. P.; Burant, J. C.; Iyengar, S. S.; Tomasi, J.; Cossi, M.; Millam, J. M.; Klene, M.; Adamo, C.; Cammi, R.; Ochterski, J. W.; Martin, R. L.; Morokuma, K.; Farkas, O.; Foresman, J. B.; Fox, D. J., **2016**.
(3) Becke, A. D. *Phys. Rev. A* **1988**, *38*, 3098-3100.
(4) Lee, C.; Yang, W.; Parr, R. G. *Phys. Rev. B* **1988**, *37*, 785-789.
(5) Becke, A. D. *J. Chem. Phys.* **1993**, *98*, 5648-5652.
(6) Krishnan, R.; Binkley, J. S.; Seeger, R.; Pople, J. A. *J. Chem. Phys.* **1980**, *72*, 650-654.
(7) Clark, T.; Chandrasekhar, J.; Spitznagel, G. W.; Schleyer, P. V. R. *J. Comput. Chem.* **1983**, *4*, 294-301.
(8) Runge, E.; Gross, E. K. U. *Phys. Rev. Lett.* **1984**, *52*, 997-1000.
(9) Bauernschmitt, R.; Ahlrichs, R. *Chem. Phys. Lett.* **1996**, *256*, 454-464.
(10) Stratmann, R. E.; Scuseria, G. E.; Frisch, M. J. *J. Chem. Phys.* **1998**, *109*, 8218-8224.
(11) Dunning, J., Thom H. *J. Chem. Phys.* **1989**, *90*, 1007-1023.
(12) Kendall, R. A.; Dunning, T. H.; Harrison, R. J. *J. Chem. Phys.* **1992**, *96*, 6796-6806.
(13) Wilson, A. K.; van Mourik, T.; Dunning, T. H. *J. Mol. Struct. Theochem.* **1996**, *388*, 339-349.
(14) Helgaker, T.; Klopper, W.; Koch, H.; Noga, J. *J. Chem. Phys.* **1997**, *106*, 9639-9646.
(15) Halkier, A.; Helgaker, T.; Jørgensen, P.; Klopper, W.; Koch, H.; Olsen, J.; Wilson, A. K. *Chem. Phys. Lett.* **1998**, *286*, 243-252.
(16) Zhong, S.; Barnes, E. C.; Petersson, G. A. *J. Chem. Phys.* **2008**, *129*, 184116.
(17) Neese, F. *WIREs Comput. Mol. Sci.* **2018**, *8*, e1327.
(18) Bannwarth, C.; Ehlert, S.; Grimme, S. *J. Chem. Theory Comput.* **2019**, *15*, 1652-1671.
(19) Bannwarth, C.; Caldeweyher, E.; Ehlert, S.; Hansen, A.; Pracht, P.; Seibert, J.; Spicher, S.; Grimme, S. *WIREs Comput. Mol. Sci.* **2021**, *11*, e1493.
(20) Pracht, P.; Bohle, F.; Grimme, S. *Phys. Chem. Chem. Phys.* **2020**, *22*, 7169-7192.
(21) Chemcraft 1.8 - graphical software for visualization of quantum chemistry computations. https://www.chemcraftprog.com (accessed 04/19/2022).
(22) Safety, S. U. E. H. https://ehs.stanford.edu/reference/information-azide-compounds, **2022**; (accessed 04/19/2022).
(23) Betzler, F. M.; Klapötke, T. M.; Sproll, S. M. *Eur. J. Org. Chem.* **2013**, *2013*, 509-514.
(24) Tischler, M.; Nasu, D.; Empting, M.; Schmelz, S.; Heinz, D. W.; Rottmann, P.; Kolmar, H.; Buntkowsky, G.; Tietze, D.; Avrutina, O. *Angew. Chem. Int. Ed.* **2012**, *51*, 3708-3712.